Available online at www.sciencedirect.com
SCIENCE DIRECT
Polymer 46 (2005) 8859–8871
polymer
www.elsevier.com/locate/polymer

Shear-induced crystallization of isotactic polypropylene within the oriented scaffold of noncrystalline ultrahigh molecular weight polyethylene

Carlos A. Avila-Orta[a,1], Christian Burger[a], Rajesh Somani[a], Ling Yang[a], Gad Marom[b], Francisco J. Medellin-Rodriguez[c], Benjamin S. Hsiao[a,*]

[a]*Department of Chemistry, State University of New York at Stony Brook, Stony Brook, NY, 11794-3400, USA*
[b]*Casali Institute of Applied Chemistry, The Hebrew University of Jerusalem, 91904 Jerusalem, Israel*
[c]*CIEP/FCQ, Universidad Autónoma de San Luis Potosí, San Luis Potosí, México*

Received 5 November 2004
Available online 1 July 2005

This paper is dedicated to the memory of Prof. John D. Hoffman

Abstract

Shear-induced crystallization of isotactic polypropylene (iPP) within the oriented scaffolds of noncrystalline ultrahigh molecular weight polyethylene (UHMWPE) was investigated by means of in situ synchrotron small-angle X-ray scattering (SAXS) and wide-angle X-ray diffraction (WAXD). The study was carried out using iPP/UHMWPE blends under isothermal crystallization at 145 °C (i.e., above the melting point of polyethylene) and step shear (shear rate = 60 s^{-1}, duration = 5 s) conditions. The oriented and isotropic iPP crystalline phases were extracted from the 2D WAXD pattern, and their kinetics data were evaluated with the Avrami equation. The dominant component in the oriented iPP phase was a kebab structure, whose nanostructure dimensions were determined by a novel SAXS analysis scheme. The minor non-crystalline but oriented UHMWPE component played a key role in the nucleation of iPP, which could be explained in terms of mutual diffusion at the interface, resulting in a significant increase in the relaxation time of iPP chains. As a result, after shear, the interfacial iPP chains could also retain their orientation and formed oriented nuclei to initiate the kebab growth.

Keywords: Shear-induced crystallization; iPP; UHMWPE

1. Introduction

Polymer crystallization from the melt has been widely studied for many decades due to its important industrial implications. However, despite the extensive research efforts [1–4] and because of the large number of variables involved in the process, the exact mechanism of flow-induced crystallization, especially at the initial stage of structure formation, is not yet fully understood. Since polymer crystallization is a kinetic event, the final morphology depends on the pathway taken, which can occur through different transient states. Variations in processing conditions and in molecular parameters of the sample have a great influence on the final morphology, and thereby on the final physical and mechanical properties.

It is known that semicrystalline polymers subjected to elongational or shear flow during melt processing often exhibit the shish-kebab structure [5,6], where the 'shish' are formed from extended chains aligned to the flow direction and are considered as primary nuclei, and the 'kebabs' are crystalline folded chain lamellae oriented perpendicularly to the flow direction. The direct consequences of mechanical deformation by flow are the induction of molecular orientation and extension, which depend on a number of processing and molecular variables, including deformation rate, strain and temperature as well as molecular weight, molecular weight distribution, chain branching and

* Corresponding author. Tel.: +1 631 632 7793; fax: +1 631 632 6518.
E-mail address: bhsiao@notes.cc.sunysb.edu (B.S. Hsiao).
[1] Present address: Centro de Investigación en Química Aplicada, Saltillo, COAH 25100, México.

0032-3861/$ - see front matter © 2005 Elsevier Ltd. All rights reserved.
doi:10.1016/j.polymer.2005.05.136

molecular architecture, etc. Recently, many experimental [7–19] and molecular dynamics simulation [20,21] studies on the early events of flow-induced crystallization of polymers have been carried out to investigate this subject. In particular, the formation of primary nuclei and the induction of nucleating scaffolds under flow are of particular interest to the community, as this area of knowledge is still relatively scarce.

The general principle for flow-induced crystallization in polymers has been clearly outlined in the past [5,15,20]. In general, application of flow (shear and elongation) induces extension of chains or chain segments along the flow direction (FD), lowering the conformational entropy and thereby reducing the free energy barrier for crystal formation. These extended chains can undergo a phase transition, including the formation of crystallization or even mesophase or transient state, which can act as nuclei to the crystallization of neighboring chains in the random coil state. In the case of long polymer chains with longer relaxation times, they are more prone to forming oriented nuclei under flow. Based on the concept of Keller et al. [5,7, 12], only a small portion of the long chains with molecular weight exceeding a critical value can remain oriented at a given flow condition. With the increase in deformation rate, more polymer chains can remain oriented after deformation. It is evident that the existence of long chains plays an important role in the formation of the precursor structure under flow, prior to the event of full-scale crystallization in polymers.

In our recent studies [7–14,17–19], isotactic polypropylene (iPP) has been chosen as a model system to understand the role of long chains in the formation of the crystallization precursor structure under shear. The iPP samples investigated included pure Ziegler–Natta iPP [10,11], blends of Ziegler–Natta iPP with low and high molecular weight [7–9], diene modified long chain branched iPP [22], and metallocene iPP in blends with atactic polypropylene (aPP) [12]. Based on experimental observations, we concluded that oriented long chains could form primary nuclei (shish), which probably were in the mesomorphic state. Recently, Li and de Jeu [13,14] demonstrated the existence of helical structures in iPP, forming smectic domains, which might act as precursors to crystallization under shear. Both research groups concluded that the flow-induced nuclei, in the form of shish, are not necessary in the crystalline state of iPP. This point of view is different from the one adopted by Kornfield and coworkers [18,19], who have also studied Ziegler–Natta and metallocene iPP samples containing bimodal blends of high and low molecular weight. The Kornfield group proposed the existence of point-like nuclei adsorbed to oriented long chains, forming 'strings' that increase the probability of long-living structures due to the increase in local orientation. The lateral lamellar growth occurs on the nuclei strings propagated perpendicular to the flow direction. This model is similar to the one proposed by Janeschitz-Kriegl et al. [23,24], in their studies of iPP crystallization under the influence of short and intense shear.

A common feature in flow induced crystallization of iPP under isothermal conditions, is that crystallization of a low molecular weight matrix can be significantly enhanced by the introduction of a small amount of higher molecular weight species [7–9,12,18,19]. In the case of polymers with narrow molecular weight distributions, such as in metallocene-based iPP, the generation of oriented nuclei under flow is hindered due to the lack of a significant amount of long chains above the overlap concentration. The presence of high molecular component is thus the key to enhance the formation of oriented nuclei in a low molecular weight matrix and its crystallization rate. To gain further insight in the role of long chains as nucleating precursors, we have investigated the role of long chains in this study. These long chain species are different from, as well as immiscible to, the chosen matrix (i.e., iPP). The chosen experimental temperature was high enough to ensure that the long-chain component was in the noncrystalline state, but the short chain matrix could undergo isothermal crystallization, where the time-resolved images from in situ small-angle X-ray scattering (SAXS) and wide-angle X-ray diffraction (WAXD) techniques could be used to follow the kebab growth and determine the growth geometry and rate, and results could be verified by the Avrami analysis [25] of the kinetics data for self-consistency check For this purpose, ultrahigh molecular weight polyethylene (UHMWPE) was selected as the long chain additive.

UHMWPE and iPP are generally considered to be immiscible in quiescent conditions [26]. Their blends have drawn attention in practical applications for the following reasons. (1) The addition of a small fraction of low molecular weight iPP can increase the fluidity [27,28] and drawability [29] of the UHMWPE matrix. (2) The addition of a small fraction of UHMWPE can increase the wear [30] and melt properties of the iPP matrix [31]. Recently, it has been suggested [31] that a small amount of UHMWPE can be microscopically dissolved into the iPP matrix, resulting in significant strain hardening under extensional flow. The use of this immiscible or partially miscible iPP/UHMWPE blend has not only allowed us to explore pathways to manipulate the nuclei scaffold under flow field, which is aimed at controlling the final morphology, but also enabled us to study the kinetics and the nature of kebab growth from the crystallizing matrix. The crystallization temperature used in this study was 145 °C. At this temperature UHMWPE does not crystallize and its relaxation times [32] are orders of magnitude higher than those of iPP.

2. Experimental

2.1. Samples and preparation

Both polymer samples were experimental materials

provided by Basell USA. Powder isotactic polypropylene (iPP), synthesized by metallocene catalysts, had a weight-average molecular weight, M_w, of 127,000 g/mol and a polydispersity of around 2. A powder ultrahigh molecular weight polyethylene (UHMWPE) sample was synthesized by the Ziegler–Natta method, having an M_w of around 6 million g/mol and a polydispersity of around 9.

Polymer blends containing up to 10 wt% of UHMWPE in iPP were prepared by solution blending [12,18,33] to ensure homogeneous mixing. Both components, weighted based on the desired composition ratio, and 5 wt% of antioxidant additive (Irgonox 1076) were then dissolved into xylene to form a solution with a concentration of about 3 wt%. The mixture was heated slowly to 120 °C with continuous stirring until a homogeneous solution was formed (the solution became transparent). The solution was kept at 120 °C for 1 h, and was subsequently poured into chilled methanol at 0 °C (5–6 times of the solution volume) under continuous stirring to precipitate the polymer mixture. The polymer blend slurry was then filtered from a xylene and methanol mixture and vacuum dried at 70 °C for at least 2 days. The same procedure was also applied to prepare a pure iPP sample. Thick polymer films (with thickness in the range of 450 ± 50 μm) were prepared by compression molding at 150 °C using a Carver pneumatic press. Samples in the form of a ring (inner diameter = 10 mm, outer diameter = 20 mm) were cut from the molded films for shear experiments.

2.2. Rheo-SAXS and rheo-WAXS measurements

An X-ray modified shear stage (based on the Linkam model CSS-450) was used to carry out the shear-X-ray experiments. A diamond window and a Kapton film were used in the modified Linkam stage. The details of this modified shear apparatus have been described elsewhere [7]. The sample was placed in the gap between the two X-ray windows. Shear was applied to the sample by rotating the bottom window while keeping the top window stationary. The experiments used a short-term shear/temperature protocol as follows [2,6,7]. The sample was first heated to 200 °C and was held for 5 min to erase the thermal history. It was subsequently cooled to 145 °C at a cooling rate of 30 °C/min. After equilibration at 145 °C, the sample was immediately subjected to a steady shear force (shear rate $\dot{\gamma} = 60\ s^{-1}$) for a duration of 5 s. In situ X-ray measurements were carried out before and after the shear (up to 1 h) at 145 °C. A control study with no shear being applied was also carried out at the same temperature.

Separate small-angle X-ray scattering (SAXS) and wide-angle X-ray diffraction (WAXD) measurements were performed at beamlines X27C and X3A2, respectively, in the National Synchrotron Light Source (NSLS), Brookhaven National Laboratory (BNL), Upton, NY, USA. In WAXD experiments, the sample-to-detector distance was 125.5 mm, calibrated by using aluminum oxide (Al_2O_3) as a standard and a wavelength of 1.54 Å. In SAXS measurements, the sample-to-detector distance was 1688.2 mm, calibrated by using silver behenate as a standard and a wavelength of 1.36 Å. An X-ray CCD camera (MAR-USA) with a resolution of 1024×1024 pixels (pixel size = 158.44 μm) was used to collect the SAXS and WAXD data. All 2D images were corrected for air scattering and beam fluctuations. The flat-plate WAXD images were corrected using the Fraser method [34] to account for the missing detection areas. The projected SAXS intensity profiles were further corrected for background scattering and the interface thickness between the crystal and amorphous phases [35].

2.3. Data analysis

2.3.1. Avrami analysis of crystallization kinetics

Shear-induced crystallization kinetics data from WAXD measurements in the early stages of the kebab formation was analyzed by the Avrami equation [25]

$$(1 - x) = \exp[-kt^n] \quad (1)$$

where x represents the crystal fraction (crystallinity), t is the crystallization time, k is the kinetics constant and n is the Avrami exponent depending on the crystal geometry, the nucleation type and the nature of crystal growth [36]. When nucleation is heterogeneous (also named predetermined or instantaneous) and the crystal growth rate is constant, the n values of 1, 2, and 3 correspond to the crystal geometry of rod, disk and sphere, respectively. On the other hand, in homogeneous nucleation (also termed sporadic nucleation) and constant crystal growth rate conditions, n values of 2, 3, and 4 correspond to the crystal geometry of rod, disk and sphere. However, the crystal growth may also be diffusion controlled (the growth rate $G(t) \propto t^{-1/2}$), which will change the interpretation of n. In typical spherulitic growth from semi-crystalline polymers, the spherulitic growth rate in the initial stages of crystallization, prior to the spherulite impingement, is often constant. This is because the crystal growth rate is substantially slower than the diffusion rate of chain mass, thus forming the rate-determined step. However, this may not be true for the kebab growth during the formation of shish-kebab structures in flow, which will be a subject of discussion in the later part of this paper.

2.3.2. Small-angle scattering from the shish-kebab structure

Recently, our laboratory has demonstrated that the SAXS data from the early stages of shear-induced crystallization can be analyzed using a shish-kebab model assuming the principle parameters with independent statistics [37]. We will briefly describe this procedure as follows. A schematic diagram of a shish-kebab assembly containing a central shish and the periodic arrangement of oriented kebabs is shown in Fig. 1. This model is assumed to have a cylindrical symmetry with the shish being the axis. The kebabs are

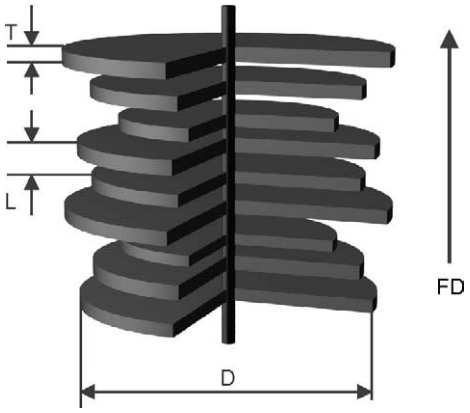

Fig. 1. The shish-kebab model containing disk-like kebabs with diameter D and thickness T and long period L.

considered round disks of diameter D and thickness T, arranged in a moderately periodic fashion with long period L. The diameter, thickness and periodicity distributions: $h_D(D)$, $h_T(T)$, and $h_L(L)$, are assumed to be statistically independent of each other. The stacking size of the kebabs is assumed infinite, and the scattering contribution of the shish is ignored. The scattering intensity of an ideal two-phase system [35] with sharp interface boundaries, free of density fluctuations within the phases, is given apart from constant prefactors like $(\rho-\rho_2)^2$, by

$$I(s_{12},s_3)s_3^2 = K[\langle|A(s_{12},s_3)|^2\rangle_{D,T} - |\langle A(s_{12},s_3)\rangle_{D,T}|^2 + |\langle A(s_{12},s_3)\rangle_{D,T}|^2|Z_L(s_3)|^2] \quad (2)$$

where $|\vec{s}| = 2\lambda^{-1}\sin\theta$, $\vec{s} = (s_1, s_2, s_3)$, $s_{12} = (s_1^2 + s_2^2)^{1/2}$ and 2θ is the scattering angle. $A(s_{12},s_3)$ represents the Fourier transform of the density distribution of a single disk of diameter D and thickness T.

$$A(s_{12},s_3) = \frac{\pi D^2}{4}\frac{2J_1(\pi D s_{12})}{\pi D s_{12}} T \frac{\sin(\pi T s_3)}{\pi T s_3} \equiv \frac{\pi D^2}{4} A_2(Ds_{12}) T A_1(Ts_3) \quad (3)$$

The abbreviated notation A_d has been introduced in a way that the index can be considered a dimension. The averages can be factorized because the dimension distributions of D and T (h_D and h_T) are assumed statistically independent:

$$|\langle A(s_{12},s_3)\rangle_{D,T}| = \langle\frac{\pi D^2}{4}A_2(Ds_{12})\rangle_D\langle TA_1(Ts_3)\rangle_T \quad (4)$$

$$\langle|A(s_{12},s_3)|^2\rangle_{D,T} = \langle\frac{\pi^2 D^4}{16}A_2^2(Ds_{12})\rangle_D\langle T^2A_1^2(Ts_3)\rangle_T \quad (5)$$

Appropriate distributions for $h_D(D)$ and $h_T(T)$, for which these averages can be carried out analytically, are given in Appendix A.

The lattice factor $|Z_L(|s_3)|^2$ can be given by

$$|Z_L(s_3)|^2 = \mathrm{Re}\left[\frac{1+H_L(s_3)}{1-H_L(s_3)}\right] \quad (6)$$

where $H_L(s_3)$ is the 1D Fourier transform of $h_L(L)$

$$H_L(s_3) = \int_0^\infty h_L(L)\exp(2\pi i L s_3)\mathrm{d}L \quad (7)$$

As in the case of $h_D(D)$, $h_T(T)$, the choice of the distribution $h_L(L)$ is also given in Appendix A. The shih-kebab model thus has 6 parameters: D, T, L, $\sigma(D)$, $\sigma(T)$ and $\sigma(L)$, where σ represents the variance.

3. Results

3.1. Wide-angle X-ray diffraction

2D WAXD images (corrected by the Fraser method [34]) of polymer blends containing different UHMWPE concentrations (0, 5 and 10 wt%) collected at 145 °C and 1 h after shear (rate = 60 s^{-1} and duration = 5 s) are illustrated in Fig. 2(a)–(c), respectively. These images are partially oriented, having a lesser degree of orientation than those collected at the early stages of crystallization. They consist

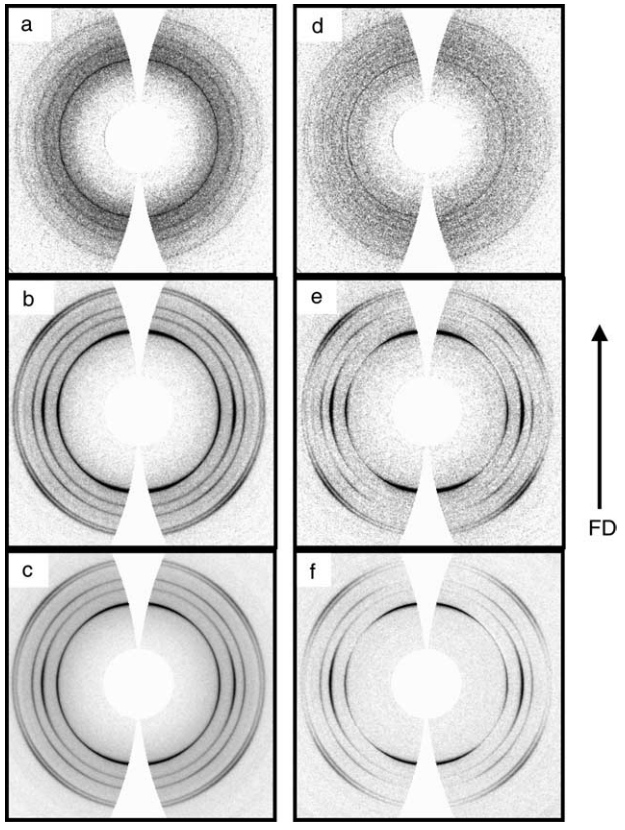

Fig. 2. 2D WAXD images (after Fraser correction) for iPP/UHMWPE blends isothermally crystallized (145 °C, 1 h) after shear ($\dot{\gamma} = 60\ s^{-1}$, duration = 5 s): (a) 0 wt%, (b) 5 wt%; and (c) 10 wt%, where (d), (e), and (f) are corresponding 2D images for the oriented fraction induced by shear. The flow direction is vertical.

of concentric diffraction rings superimposed with sharp diffraction arcs, indicating the coexistence of oriented and non-oriented (isotropic) crystalline fractions in the sheared sample after 1 h of annealing. An image analysis method [38], introduced previously by our laboratory, was used to determine the contribution of each phase in the 2D WAXD image. As an example, corresponding 2D WAXD images of the oriented phase in the three samples extracted from the initially measured Fraser corrected images, are shown in Fig. 2(d)–(f).

The 1D intensity profiles of oriented and isotropic fractions were integrated azimuthally from the corresponding 2D deconvoluted patterns. Typical results from the iPP/UHMWPE (90/10) blend at 1 h after shear are shown in Fig. 3(a), where the total, oriented and isotropic 1D intensity profiles are shown. It is seen that the sheared blend exhibited a dominant α-crystal form [39] and a small fraction of the γ-crystal form [40] (its characteristic is marked by the appearance of the (117) reflection), which was observed in all three samples (100/0, 95/5 and 90/10) as shown in Fig. 3(b). The γ-crystalline phase appears to be the characteristic of metallocene synthesized iPP due to regio defects of the chain [40]; it is also present only in the isotropic phase. In Fig. 3, it is clear that, under the chosen experimental conditions (145 °C), only iPP crystallizes, whereas the UHMWPE component remains in the amorphous state.

The crystalline and amorphous contributions of oriented and isotropic fractions (Fig. 3(a)) were obtained from the integrated intensity profiles using by the 1D peak deconvolution method [12]. The oriented fraction consists of oriented crystal phase ($x_{C,I}$) and oriented amorphous phase ($x_{A,O}$), while the isotropic fractions consist of isotropic crystal phase ($x_{C,I}$) and isotropic amorphous phase ($x_{A,I}$). The time evolution profiles of total (x_C) oriented and non-oriented ($x_{C,O}$ and $x_{C,I}$) crystalline

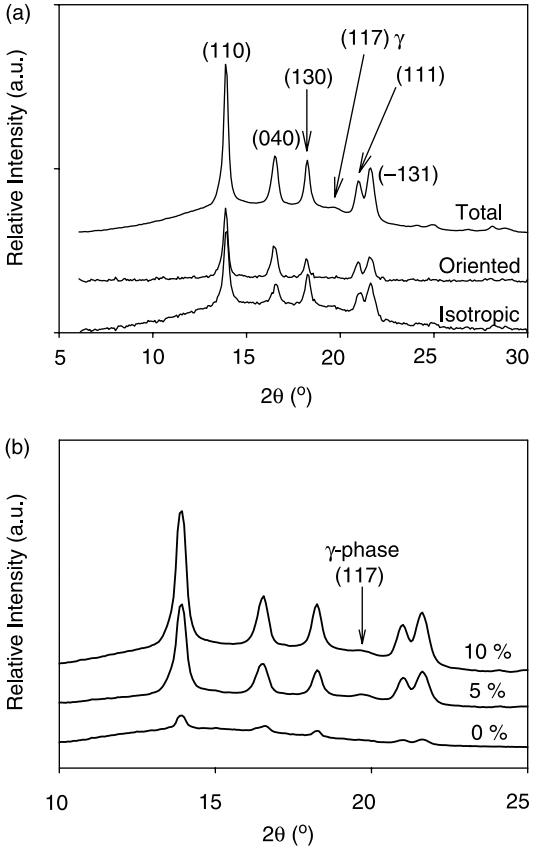

Fig. 3. (a) Integrated 1D WAXD profiles of total, oriented and isotropic phases for the iPP/UHMWPE (90/10) blend, isothermally crystallized (145 °C, 1 h) after shear ($\dot{\gamma} = 60\ s^{-1}$, duration = 5 s). (b) 1D integrated WAXD intensity profiles for three iPP/UHMWPE samples.

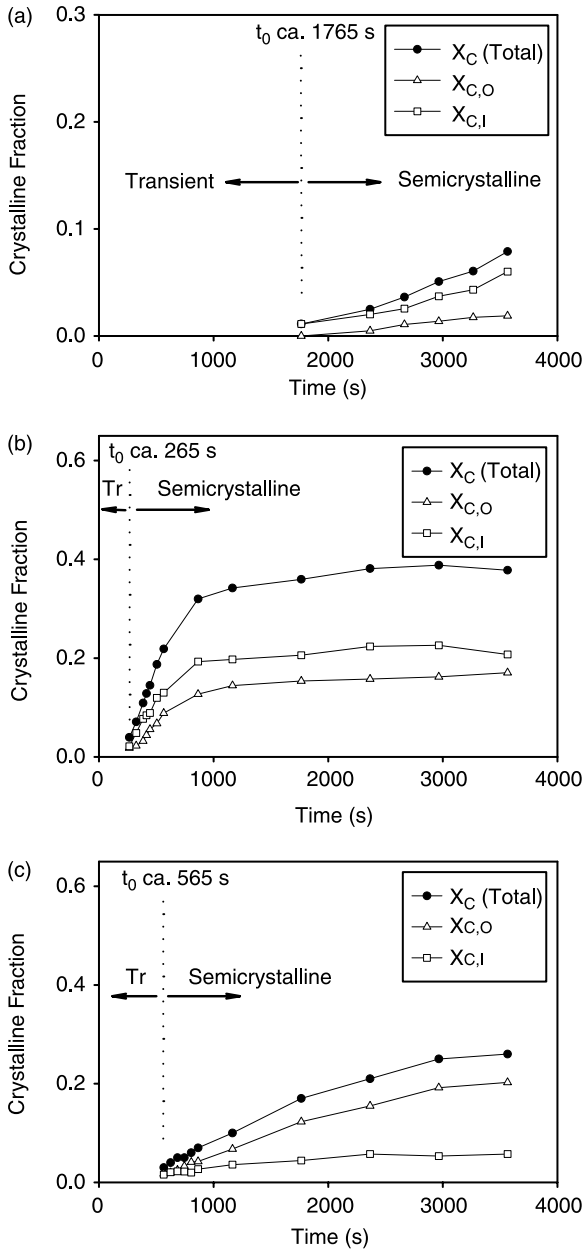

Fig. 4. Crystallinity evolution for iPP/UHMWPE blends isothermally crystallized (145 °C, 1 h) after shear ($\dot{\gamma} = 60\ s^{-1}$, duration = 5 s) for (a) 0, (b) 5, and (c) 10 wt% UHMWPE samples.

fractions for three samples at 145 °C are shown in Fig. 4. It is seen that both oriented and non-oriented ($x_{C,O}$ and $x_{C,I}$) crystalline fractions tracked the same time-evolution trend as the total crystalline fraction (x_C). The crystallization induction time for both iPP/UHMWPE blends decreased by about 6 times as compared with that of pure iPP (however the 10 wt% UHMWPE blend was found to have a slower induction time than the 5 wt% blend, which will be explained later). In addition, higher crystallinity and faster kinetics were observed in the iPP/UHMWPE blends. The values of crystallization induction time, t_0, were determined by WAXD for iPP and the 5 and 10 wt% UHMWPE blends were 1765, 265 and 565 s, respectively.

As we are particularly interested in the development of the oriented crystalline fraction in iPP, which directly reflects the effect of shear-induced oriented noncrystalline UHMWPE scaffold on the crystallization of the iPP matrix, the time evolution data of $x_{C,O}$ was analyzed by the Avrami method (Eq. (1)). Fig. 5 illustrates the double-logarithmic Avrami plot of the oriented fractions for three samples. It is interesting to note that in pure iPP, only one slope was seen, corresponding to primary crystallization. This suggests that secondary crystallization in pure iPP was not present under the chosen experimental conditions; it would probably appear at long crystallization times beyond the time frame of this study. However, this is not the case in the blend samples, where two slopes were seen. The Avrami parameters, n and k, of oriented iPP crystals for pure iPP and the iPP/UHMWPE blends are shown in Table 1. It is seen that the k values of the blends are significantly larger than those of pure iPP, indicating that the presence of UHMWPE has a large influence on the crystallization kinetics of the oriented phase. However, the k value of the 5 wt% sample was found to be slightly larger than that of the 10 wt%. In Table 1, all three samples exhibited the value of $n \approx 2$, suggesting that there are several possible growth geometries at the initial stage of shear-induced crystallization in iPP/UHMWPE blends and pure iPP matrix: the

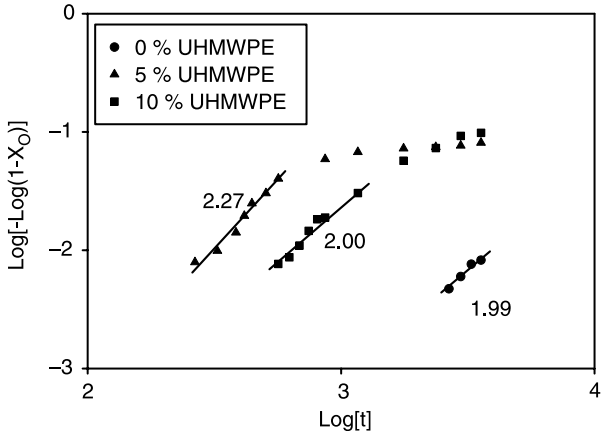

Fig. 5. Avrami plots for iPP/UHMWPE blends isothermally crystallized (145 °C, 1 h) after shear ($\dot{\gamma} = 60\ s^{-1}$, duration = 5 s) for the growth of oriented crystal fraction.

Table 1
Avrami parameters n and k for iPP/UHMWPE blends isothermally crystallized at 145 °C after shear ($\dot{\gamma} = 60\ s^{-1}$, shear duration = 5 s)

% UHMWP-E	Oriented fraction		
	$k_O/10^{-8}$, s^{-1}	n_O	Growth geometry
0	0.74	2.0	Disk
5	27.54	2.3	Disk
10	23.99	2.0	Disk

k_O, rate constant for the oriented phase. n_O, Avrami exponent for the oriented phase.

1D rod-like growth with a constant velocity, or the 2D disk-like growth with a diffusion-controlled velocity ($G(t) \propto t^{-1/2}$), both under spontaneous nucleation conditions. The latter condition has been verified as the correct mechanism, which will be discussed later (G was calculated from the time-evolution of the kebab formation based on the SAXS data).

3.2. Small-angle X-ray scattering

The lamellar morphology of iPP/UHMWPE blends formed during the isothermal crystallization at 145 °C after shear ($\dot{\gamma} = 60\ s^{-1}$, 5 s) was determined by means of SAXS. Of particular interest is the morphology formed prior to the value of t_0 (as shown in Fig. 4), since it can provide information regarding the precursor structures of iPP developed during the transient stage. Selected 2D SAXS images (below, near and above t_0) for iPP, 5 and 10 wt% UHMWPE blends, are shown in Figs. 6–8, respectively. In Fig. 6, a distinct two-point pattern was seen, showing the characteristics of oriented lamellae grown perpendicularly to the flow direction. In the case of samples with UHMWPE (Figs. 7 and 8), the presence of a weak equatorial streak was seen at the transient state, while a strong meridional streak was seen later at time t_0 (pattern b of Fig. 6), which was a clear indication of the shish-kebab structure [37]. At times larger than t_0, the appearance of a meridional streak changed into a two-point pattern.

The value of long period L along the meridian direction at $t > t_0$ was calculated from the position of the scattering maximum using Bragg's law. The evolution of L with time for iPP and iPP/UHMWPE blends crystallized isothermally at 145 °C after shear ($\dot{\gamma} = 60\ s^{-1}$, 5 s) is illustrated in Fig. 9. It was seen that the L value of pure iPP remained constant throughout the transient and crystallization stages; whereas the L value decreased in the transient stage for the blends, and then reached a plateau at the crystallization stage. The periodicity of iPP was slightly increased with addition of UHMWPE.

The 2D-SAXS images obtained prior to t_0 were subjected to a more detailed analysis. In an attempt to determine the size and evolution of the shish-kebab structures prior to the crystallization induction time ($t < t_0$), 2D SAXS meridional

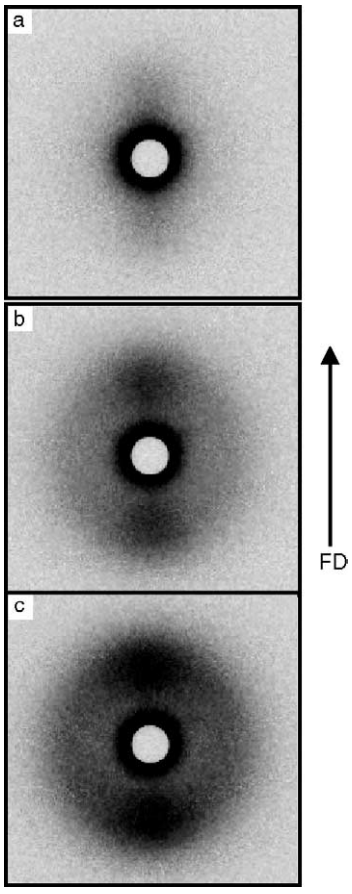

Fig. 6. 2D SAXS images for iPP isothermally crystallized (145 °C) after shear ($\dot{\gamma} = 60\ s^{-1}$, duration = 5 s) at (a) 580 s, (b) 1780 s and (c) 3580 s.

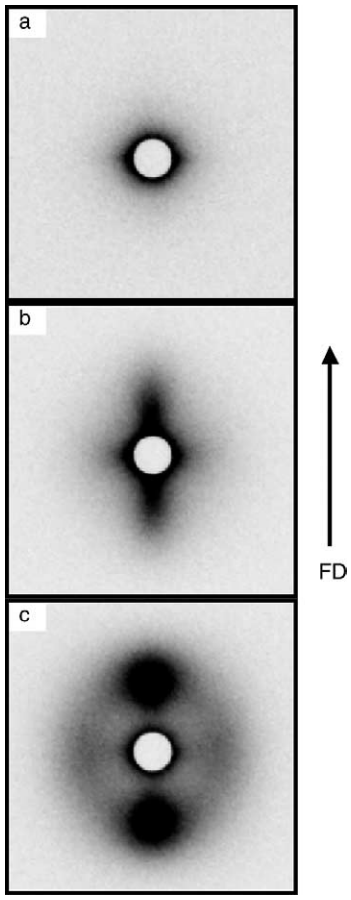

Fig. 7. 2D SAXS images for iPP/UHMWPE blends (95/5) isothermally crystallized (145 °C) after shear ($\dot{\gamma} = 60\ s^{-1}$, duration = 5 s) at (a) 55 s, (b) 280 s and (c) 3580 s.

profiles were fit by the shish-kebab scattering model [37]. In this fit, oriented disk-like kebabs (Fig. 1) characterized by the disk thickness T, disk diameter D and distance between disks (long period) L, as well as by their distributions, were modeled by using the general expression in Eq. (2). An example of this model fit to a set of experimental data is shown in Fig. 10, where a series of meridional profiles and their fits are superimposed. The fit results for the three samples at selected times are presented in Table 2. In general, the disk thickness and disk diameter increase with time, while the long period decreases slightly.

4. Discussion

Crystallization kinetics and lamellar morphology of iPP at 145 °C after a step shear ($\dot{\gamma} = 60\ s^{-1}$, 5 s) are affected by the presence of UHMWPE. Results in the previous section show the following pathways towards the development of final morphology: (1) the initial presence of amorphous melt for both iPP and UHMWPE components at $t = 0$, (2) the initiation of iPP precursor structure in the transient state by the presence of oriented UHMWPE chains at $t < t_0$, and (3)

Table 2
Morphological parameters for oriented kebabs for the precursor structure in the transient state of iPP/UHMWPE blends, isothermally crystallized at 145 °C after shear ($\dot{\gamma} = 60\ s^{-1}$, duration = 5 s)

Time (s)	T (nm)	D (nm)	L (nm)	σ_T (nm)	σ_D (nm)	σ_L (nm)
	IPP					
580	5.6	16.7	25.5	2.6	7.0	7.0
880	6.5	19.4	24.8	2.3	5.0	6.7
1180	9.7	24.3	22.8	2.6	2.3	7.0
	iPP/UHMWPE (95/5 wt/wt%)					
55	4.3	6.7	30.1	2.1	3.0	10.7
	iPP/UHMWPE (90/10 wt/wt%)					
55	5.9	17.7	32.9	3.3	10.0	9.5
130	14.0	35.0	32.3	2.4	7.0	11.9

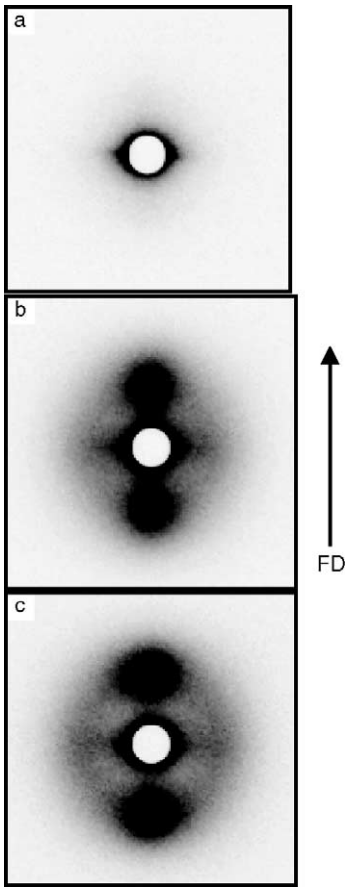

Fig. 8. 2D SAXS images for iPP/UHMWPE blends (90/10) isothermally crystallized (145 °C) after shear ($\dot{\gamma} = 60\ s^{-1}$, duration = 5 s) at (a) 55 s, (b) 580 s and (c) 3580 s.

the crystallization of iPP within the oriented UHMWPE scaffolds at $t > t_0$. The isotropic ipp melt consists of a random coil configuration. The precursor state of iPP contains oriented iPP chains developed first as nuclei, probably in the mesomorphic form [10], and subsequent development of crystalline kebab structures with low crystallinity (i.e., the shish-kebab structure). Formation of

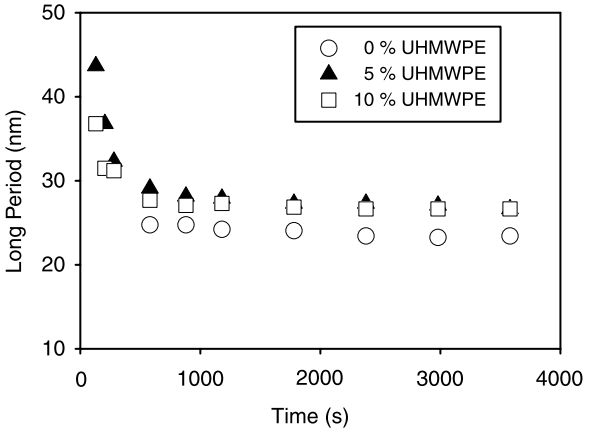

Fig. 9. Periodicity evolution for iPP/UHMWPE blends isothermally crystallized (145 °C, 1 h) after shear ($\dot{\gamma} = 60\ s^{-1}$, duration = 5 s).

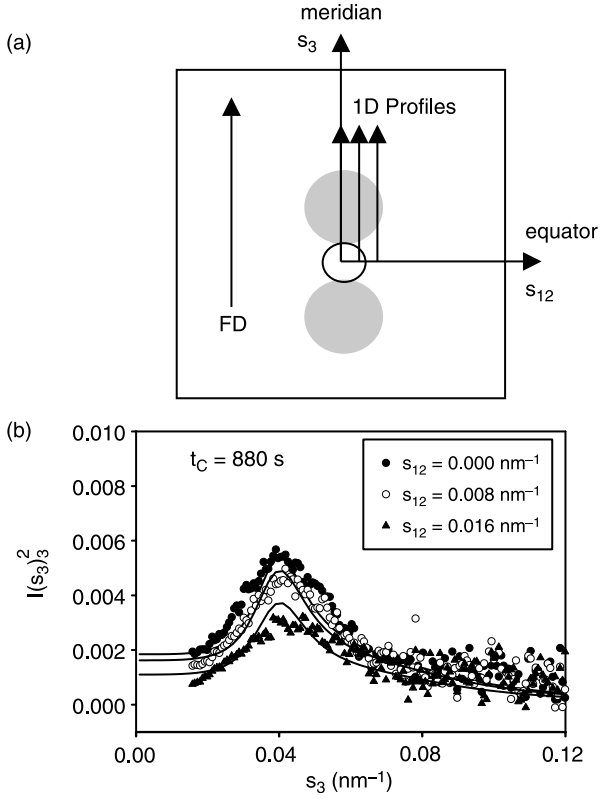

Fig. 10. 1D intensity profiles $I(s_3)$ extracted from 2D SAXS profiles at constant s_{12} fitted by the shish-kebab model: (a) schematic diagram of the intensity profile extraction, (b) experimental profiles and the shish-kebab model fit using the data from pure iPP isothermally crystallized (145 °C, 880 s) after shear ($\dot{\gamma} = 60\ s^{-1}$, duration = 5 s).

semicrystalline morphology in iPP proceeds from such a precursor structure. The crystallization induction time, t_0, can be considered as a 'characteristic time' defining the limit between the transient state and the crystallization process.

It is seen that the crystallization induction time, t_0, depends on the UHMWPE content (Fig. 4): 1765, 265, and 565 s for UHMWPE concentrations of 0, 5 and 10 wt%, respectively. The addition of 5 wt% of UHMWPE exhibited the lowest induction time because further increase of UHMWPE in fact delayed the crystallization process. Based on this observation, we argue that the dynamics of the precursor structural formation at $t < t_0$ is related to both phase behavior and viscoelastic (relaxation) property of the UHMWPE component in the blend.

4.1. Phase behavior in the melt

It is well documented that melt crystallization in polymer blends can undergo complicated phase transitions [41] due to competition between the kinetics of phase separation and the thermodynamic driving force. The level of molecular mixing, known as the miscibility, can play a critical role in the development of non-equilibrium structures in the final products [42,43]. In binary blends, the blend components in

the molten state can be miscible in the entire composition range, partially miscible and immiscible. In the system with partial miscibility, the blend can exhibit lower critical solution temperature (LCST) and/or upper critical solution temperature (UCST) [43], where both values are affected by the introduction of flow [44,45]. In the case of LCST behavior, phase dissolution can be induced by high shear rate (i.e., the LCST increases with shear rate), while phase separation is more favorable at lower shear rates [44].

In iPP and PE blends, some groups considered these two components to be immiscible [46,47], while others reported some partial miscibility between them in the molten state [26,48,49]. Based on the Flory–Huggins theory, the iPP/PE blends, with relatively low molecular weight components, should exhibit a UCST phase diagram having a critical point of 143 °C. Thus, a single phase should appear above 137 and 133 °C for blends with 10 and 5 wt% PE, respectively. In the case of UHMWPE, the immiscibility region would be significantly enhanced. However, as the UHMWPE component was kept at relatively low ratios (5 and 10 wt%), we believe that some levels of interaction between the supercooled iPP and amorphous UHMWPE chains should exist [31] in the chosen blend. This would be consistent with the study showing that the drawability of iPP/UHMWPE was enhanced by the entangled mesh between iPP and UHMWPE [29].

Based on the above considerations, we might consider that the blend components were at least partially miscible in the melt at 145 °C. Thus, it is logical to consider a three-phase system in the sheared melt prior to crystallization, i.e., the iPP phase, the UHMWPE phase, and the interface region, where the two components are partially miscible. However, according to the phase diagram, we expect that the degree of phase separation in the 10 wt% blend will be larger than that in the 5 wt% blend.

4.2. Chain relaxation in the blend

In pure iPP, only a small fraction of oriented chains acted as effective nuclei, while most of the chains relaxed to the random coil state. In the case of blends with UHMWPE, the fraction of oriented iPP chains that could act as effective nuclei were greatly increased due to the presence of UHMWPE. This can be explained by the mutual diffusion between the iPP and UHMWPE chains at the interface, as follows. Reptation of chains within a tube created by surrounding chains is the main mechanism for diffusion and relaxation of linear entangled polymers [50,51]. Other mechanisms, not taken into account in the original formulation of reptation theory, such as contour length fluctuations [52] and constraint release [53], would also affect the relaxation of entangled linear polymers. In particular, constraint release (i.e., the lateral motion of the chain out of its original tube because of the motion of surrounding chains) is important for polydisperse melts because fast motions of short chains allow more rapid partial relaxation of long chains to remove the topological barriers. Double reptation [54], involving two chains entangled at a fixed stress point, is a concept frequently adopted to compensate for constraint release. It is thought that the entanglement relaxes when the end of either chain passes through. Double reptation is useful in describing the faster relaxation of long chains due to the presence of shorter chains, and vice versa, i.e., short chains relax slower by the presence of long chains. However, in some cases, the reptation behavior of short chains remains unchanged in blends, and long chains dominate the relaxation behavior. This can occur due to tube dilation [55] in the reptation of long chains; where for short chains the tube does not dilate (the relaxation time of short chains is the same in the pure melt and in the blend). In the case of long chains, tube dilation takes place in the blend and the relaxation behavior has to account for this effect [56]. A detailed analysis of the relaxation behavior of iPP/UHMWPE blends is beyond the scope of this study. However, the ratio of relaxation times of long and short chains was estimated by simple means as a guide to explain the X-ray results.

Theoretically, the relaxation times of pure melts [56] can be obtained when $M_L > M_S > M_e$ (M_L, M_S, and M_e: molecular weight for long chains, short chains and entanglements, respectively) by means of

$$\tau_L \propto M_L^3 \tag{8}$$

$$\tau_S \propto \tau_L \left(\frac{M_S}{M_L}\right)^3 \propto M_S^3 \tag{9}$$

where τ_L and τ_S are the relaxation times for long and short chains, respectively. Eq. (9) can be used to estimate the relaxation times of short chains in the blend, assuming that the relaxation behavior is the same as in the pure melt. The ratio of the reptation time of the long chains in an undiluted tube to the constraint release Rouse time [57] known as the Graessley parameter, Gr, can be used to determine whether tube dilation for long chains occurs or not. It is given by

$$\mathrm{Gr} = M_L M_e^2 / M_S^3 \tag{10}$$

assuming contour length fluctuations are neglected. If Gr is much smaller than a critical value, $\mathrm{Gr},c = 0.064$, long chain motion in binary blends can be predicted using reptation in the undiluted tube [57]. We estimated $\mathrm{Gr} = 0.0037$ for the iPP/UHMWPE blend components in this study (using their weight-average molecular weights), falling in the range of the undiluted tube. Tube dilation for UHMWPE chains may occur for M_e higher than 5000, which is likely to occur due to the presence of iPP short chains. Nevertheless, relaxation time for long chains can be cautiously estimated using Eq. (9). Using the reported values in the experimental section for M_W of iPP (M_S) and UHMWPE (M_L), the ratio τ_L/τ_S was estimated $\approx 64{,}000$. On the other hand, it is well known that the relaxation time of polymer chains in the melt is proportional to the molecular weight scaled to 3.4 ($\tau \propto M_w^{3.4}$) as

determined by a number of experiments [12]. In this case, the ratio τ_L/τ_S would be approximately 280,000. In any case, double reptation will prevail here, causing the relatively short iPP chains to relax much more slowly by the presence of long UHMWPE chains in the blend than those in pure iPP.

Based on the above consideration, long UHMWPE chains would retain orientation after shear, which also promotes the orientation of the surrounding iPP chains due to the increased relaxation time. The oriented iPP chains can serve as effective nuclei for the further crystallization of unoriented iPP chains, thus significantly enhancing the crystallization kinetics. This is consistent with the large decrease in the induction time of crystallization and the increase in high temperature crystallinity in the blends, as shown in Fig. 4. In this figure, it is interesting to see that the crystallization kinetics of the 5 wt% blend is faster than that of the 10 wt% blend, and the high temperature crystallinity of the 5 wt% blend is higher than that of the 10 wt% blend. This behavior is perhaps due to the higher degree of phase separation between iPP and UHMWPE in the 10 wt% blend, which effectively decreases the interfacial interactions between iPP and UHMWPE chains. In other words, the component of UHMWPE in the 10 wt% blend is less effective in promoting the orientation and stretching of iPP chains at the interface.

It is necessary to point out that the above experiments were carried out at constant shear rate and strain. Thus, the pure iPP and iPP/UHMWPE blends would experience different shear stresses because of the differences in their rheological responses (the bulk stress of the iPP/UMMWPE blend would be higher). Thus, another viewpoint to explain the above finding can be attributed to higher stress and higher concentration of iPP chain-stretching exerted, resulting in a higher concentration of shish in the blend than in pure melt. However, the coupled phase separation still played an important role on the final crystallization process, as seen in the minimum of the induction time.

4.3. Shear-induced nuclei scaffolds

In pure polymer melt, nuclei scaffolds (i.e., network of oriented crystallization precursor structures [10,17]), consisting of primary nuclei (shish) with long connectivity and 'kebab' crystals induced by 'shish' with poor lateral connectivity, can be generated by the application of shear. In the iPP/UHMWPE blend, we envision that the shear-induced nuclei scaffolds are created in a similar fashion, except that the creation of shish is associated with the formation of oriented UHMWPE chains in the interface. In other words, the formation of oriented UHMWPE scaffolds induced by shear, even though they are non-crystallizable, would define the landscape of oriented iPP nuclei surrounding the iPP/UHMWPE interface.

At the initial stage of the scaffold formation ($t < t_0$), no crystalline structures in the blend was seen by WAXD. However, their oriented structures were detected by SAXS (for example, in Fig. 7(a) and (b), equatorial streaks were observed immediately after shear). The appearance of scattering features in SAXS prior to WAXD has also been observed in iPP [58] and other polymers [59] in the past. Different reasons have been attributed to this behavior: (1) the low detection limit of WAXD, (2) defective initial crystal order, (3) shish largely consisting of a mesophase structure, and (4) periodic axial density variation within the shish. It is believed that all of them can contribute to the appearance of SAXS patterns before WAXD crystalline signals.

The morphological development of the precursor structure in the transient state can be obtained by qualitative and quantitative analyses of the 2D SAXS images for pure iPP and 5 and 10 wt% UHMWPE blends collected after shear (Figs. 6–8). In pure iPP, the SAXS image collected immediately after shear did not exhibit any discernible scattering feature. At longer times, a pair of weak meridional scattering peaks was seen (e.g. Fig. 6(a)), indicating the development of lamellar structures (or kebabs without shish). The lack of shish detection (as in the form of equatorial streak) by SAXS did not indicate that the shish entity was not present in the shear melt, rather it suggested that the formed shish may be too small or too diluted to be detected by SAXS. In iPP/UHMWPE blends, SAXS images collected immediately after shear (Figs. 7(a) and 8(a)) showed distinct equatorial streaks, indicating the formation of a sizable fibrillar structure along the flow direction. As there was no sign of WAXD crystal diffraction, this shish structure may consist of defective iPP extended chain crystals [15,59] and/or bundles of mesomorphic chains [7–12] that can act as primary nuclei for secondary crystallization of folded-chain lamellae. We believe the hypothesis of mesomorphic shish in iPP is more reasonable, which is also consistent with the recent study of smectic filaments in shear iPP melts that act as nuclei stabilizers by de Jeu et al. [13,14]. The large shish dimension observed in SAXS is consistent with the 'decoration' process of forming an mesomorphic iPP layer at the interface of UHMWPE, outlining the contour of the oriented non-crystallization UHMWPE scaffolds.

At later times in the transient stage, a strong meridional streak, which was subsequently converted into a pair of meridional peaks, was developed on top of the equatorial streak. The appearance of weak equatorial streak and strong meridional streak/peaks (Figs. 7(b) and 8(b)) is the characteristic of 'shish-kebab' morphology, where kebabs grow normal to the flow direction having a cylindrical symmetry around the shish. The generation of less thermodynamically stable folded-chain kebab lamellae from the partial surface of more thermodynamically stable extended-chain shish strongly favors the mechanism of kebab formation by adsorption of lamellae on the shish as proposed by Muthukumar et al. [21], rather than the conventional arguments based on the epitaxial growth of

lamellae around the shish or the initiation of the free chain ends (cilia)/protrudes from the central shish surface.

The detailed iPP kebab morphology, developed at the transient stage, can be described quantitatively by the use of the shish-kebab model (Fig. 1) to fit the 2D SAXS pattern. The structural parameters of kebabs for pure iPP and iPP/UHMWPE blends developed at selected times prior to crystallization (detected by WAXD) are shown in Table 2 (note that these kebabs consist of folded-chain lamellae, however its total crystallinity is too low (<1 wt%) to be detected by WAXD). It was seen that the spatial arrangement of the kebab assembly was relatively loose (L is in the range of 20–30 nm, which is in good agreement with results from Fig. 9) and the average thickness (T) of the kebab entities was relatively thin (less than 10 nm). In both pure and blend samples, the L value was found to decrease with time, which can be attributed to the formation of new kebabs; the T value was found to increase with time, which can be attributed to the lamellar perfection process. The growth of the lamellar disk (D, in the range of about 10–30 nm) was found not to be linear with time, which indicated the initial kebab growth did not have a constant rate. Instead, the lamellar growth rate appeared to follow the diffusion controlled process (i.e. the kebab growth rate, G, is proportional to $t^{-1/2}$). This will be the subject of a detailed study later. The above conclusion is certainly consistent with results from our earlier Avrami analysis, where $n=2$ may represent the sporadic nucleation of disk-like crystal geometry with diffusion controlled growth for both pure iPP and iPP/UHMWPE blends. It was also found that the L period in the blend was generally larger than that in pure iPP, which is consistent with the longer iPP shish dimension generated by the presence of large oriented UHMWPE scaffolds.

4.4. Crystallization within the oriented nuclei scaffolds

Isothermal crystallization of iPP in the oriented nuclei scaffolds can be viewed as a decoration process of folded-chain crystallization from coiled chains within the nuclei landscape predetermined with the density of the nuclei, the dimension of the nuclei and the orientation of the nuclei. The growth rate and the thickness of iPP lamellae are primarily dictated by the experimental temperature, not by the shear condition or the UHMWPE content. It is generally true that the addition of UHMWPE can significantly enhance the crystallization rate due to the increase of iPP nuclei density, at the interface region between iPP and UHMWPE. However, it was clear that the increase in the UHMWPE content did not further enhance the crystallization kinetics or the high temperature crystallinity (for example, the comparison between the 5 and 10 wt% blends in Figs. 4 and 5). This can be attributed to the enhanced phase separation in the blend with the higher content of UHMWPE. As the large UHMWPE domain is formed, the effective interface between iPP and UHMWPE chains can be decreased, resulting in a lesser effect to impact the shear-induced crystallization.

5. Conclusions

The effect of UHMWPE in shear-induced crystallization of iPP at 145 °C was studied by means of synchrotron SAXS and WAXD techniques. Under the experimental conditions, UHMWPE remained noncrystalline but formed an oriented scaffolding structure, which induced iPP nucleation and growth. Three stages were recognized in the shear-induced crystallization process of iPP/UHMWPE blends: (1) amorphous melts of partially miscible blends before shear, (2) formation of oriented noncrystalline UHMWPE scaffolds and mesomorphic/crystalline iPP nuclei at the interface, and (3) crystallization of iPP within the nuclei scaffolds. The enhanced iPP nuclei formation by UHMWPE chains can be explained by the double reptation theory, where the relaxation times of the iPP chains at the iPP/UHMWPE interface become significantly retarded, enabling the retention of molecular orientation after shear and the formation of oriented nuclei. As a result, the presence of UHMWPE chains affects the crystallization kinetics and the high temperature crystallinity of iPP induced by shear. However, the increase of the UHMWPE content promotes phase separation between iPP and UHMWPE, leading to a lesser nucleating effect.

Acknowledgements

This study was supported by the NSF Inter-American Grant (DMR0302809) and NSF (DMR9984102) at Stony Brook. The SAXS synchrotron beamline X27C was supported by the Department of Energy (Grant DE-FG02-99ER 45760). The Israeli member (GM) was supported by the Israel Science Foundation (Grant No. 40/01). CAAO acknowledges the postdoctoral fellowship granted by CONACYT (México).

Appendix A

Appendix A1. Choice of h_D and h_T

A bell-shaped distribution for both $h_D(D)$ and $h_T(T)$, where the required averages can be calculated analytically, is given by (X replaces D and T, respectively)

$$h_X(X) = \frac{2}{\Gamma(\nu_X)X_0}\left(\frac{X}{X_0}\right)^{2\nu_X-1}\exp\left[-\left(\frac{X}{X_0}\right)^2\right] \tag{A1}$$

with moments

$$\langle X^n\rangle_X = \frac{\Gamma(\nu_X + n/2)X_0^n}{\Gamma(\nu_X)} \tag{A2}$$

$$\langle X\rangle_X = \frac{\Gamma(\nu_X + 1/2)X_0}{\Gamma(\nu_X)} \tag{A3}$$

$$\langle X^2\rangle_X = \nu_X X_0^2 \tag{A4}$$

$$\langle X^4\rangle_X = \nu_X(1+\nu_X)X_0^2 \tag{A5}$$

The parameters X_0 and ν_X need to be evaluated by numerical iteration for a given center X and standard deviation σ_X. The required averages are given as follows (for simplicity ν_X is replaced by ν).

$$\left\langle \frac{\pi^{d/2}X^d}{2^d\Gamma(1+d/2)} A_d(Xs)\right\rangle_X = \frac{\pi^{d/2}\Gamma(\nu+d/2)X_0^d}{2^d\Gamma(\nu)\Gamma(1+d/2)}\,{}_1F_1^1\left(\begin{matrix}\nu+d/2\\ 1+d/2\end{matrix}\middle| -\frac{\pi^2X_0^2s^2}{4}\right) \tag{A6}$$

$$\left\langle \frac{\pi^{d}X^{2d}}{4^d[\Gamma(1+d/2)]^2} A_d^2(Xs)\right\rangle_X = \frac{\pi^{d}\Gamma(d+\nu)X_0^{2d}}{4^d\Gamma(\nu)[\Gamma(1+d/2)]^2} \times {}_2F_2^2\left(\begin{matrix}(1+d)/2, d+\nu\\ 1+d/2, 1+d\end{matrix}\middle| -\frac{\pi^2X_0^2s^2}{4}\right) \tag{A7}$$

$$\langle TA_1(Ts_3)\rangle_T = \frac{\Gamma(\nu+1/2)T_0}{\Gamma(\nu)}\,{}_1F_1^1\left(\begin{matrix}\nu+1/2\\ 3/2\end{matrix}\middle| -\frac{\pi^2T_0^2s_3^2}{4}\right) \tag{A8}$$

$$\left\langle \frac{\pi D^2}{4} A_2(Ds_{12})\right\rangle_D = \frac{\pi\nu D_0^2}{4}\,{}_1F_1^1\left(\begin{matrix}1+\nu\\ 2\end{matrix}\middle| -\frac{\pi^2D_0^2s_{12}^2}{4}\right) \tag{A9}$$

$$\langle T^2A_1^2(Ts_3)\rangle_T = \frac{\left[1 - {}_1F_1^1\left(\begin{matrix}\nu\\ 1/2\end{matrix}\middle|{-\pi^2T_0^2s_3^2}\right)\right]}{2\pi^2s^2} \tag{A10}$$

$$\left\langle \frac{\pi^2D^4}{16} A_2^2(Ds_{12})\right\rangle_D = \frac{\pi^2\nu(1+\nu)D_0^4}{16}\,{}_2F_2^2\left(\begin{matrix}3/2, 2+\nu\\ 2, 3\end{matrix}\middle|{-\pi^2D_0^2s_{12}^2}\right) \tag{A11}$$

where ${}_1F_1$ is the confluent hypergeometric function and ${}_2F_2$ is a generalized hypergeometric function.

Appendix A2. Choice of h_L

The use of a Γ-distribution is recommended when the stacking periodicity is highly disordered (σ_L is large) to eliminate an unphysical tail of the distribution at negative values expected in the Gaussian case. The following G-distribution can be used

$$h_L(L) = \frac{1}{\Gamma(\nu_L)L_0}\left(\frac{L}{L_0}\right)^{\nu_L-1}\exp\left(-\frac{L}{L_0}\right) \tag{A12}$$

The Fourier transform of the Γ-distribution is given by

$$H_L(s_3) = (1 - 2\pi i L_0 s_3)^{-\nu_L} \tag{A13}$$

where the parameters L_0 and ν_L depend on center L and standard deviation σ_L as $L_0 = \sigma_L^2/L$ and $\nu_L = L^2/\sigma_L^2$.

References

[1] Hoffman JD, Davis GT, Lauritzen Jr JI. In: Hannay NB, editor. Treatise on solid state chemistry, vol. 7. New York: Plenum; 1976 [chapter 7].
[2] Eder G, Janeschitz-Kriegl H, Liedauer S. Prog Polym Sci 1990;15:629.
[3] Armitstead K, Goldbeck-Wood G. Adv Polym Sci 1992;100:219.
[4] Strobl G. Eur Phys J E 2004;3:165.
[5] Keller A, Kolnaar HWH. Mater Sci Technol 1997;18:189.
[6] Eder G, Janeschitz-Kriegl H. Mater Sci Technol 1997;18:268.
[7] Somani RH, Hsiao BS, Nogales A, Srinivas S, Tsou AH, Sics I, et al. Macromolecules 2000;33:9385.
[8] Somani RH, Hsiao BS, Nogales A, Fruitwala H, Srinivas S, Tsou A. Macromolecules 2001;34:5902.
[9] Nogales A, Hsiao BS, Somani RH, Srinivas S, Tsou AH, Balta-Calleja FJ, et al. Polymer 2001;42:5247.
[10] Somani RH, Yang L, Hsiao BS, Agarwal PK, Fruitwala H, Tsou A. Macromolecules 2002;35:9096.
[11] Somani RH, Yang L, Hsiao BS. Physica 2002;A304:145.
[12] Somani RH, Yang L, Hsiao BS, Fruitwala H. J Macromol Sci Phys 2003;B42:515.
[13] Li L, de Jeu WH. Macromolecules 2003;36:4862.
[14] Li L, de Jeu WH. Phys Rev Lett 2004;92:075506.
[15] Hobbs JK, Humphris ADL, Miles MJ. Macromolecules 2001;34:5508.
[16] Hobbs JK, Miles MJ. Macromolecules 2001;34:353.
[17] Pogodina NV, Lavrenko VP, Srinivas S, Winter HH. Polymer 2001;42:9031.
[18] Seki M, Thurman DW, Oberhauser JP, Kornfield JA. Macromolecules 2002;35:2583.
[19] Kornfield JA, Kumaraswamy G, Issaian AM. Ind Eng Chem Res 2002;41:6383.
[20] Hu W, Frenkel D, Mathot VBF. Macromolecules 2002;35:7172.
[21] Dukovski I, Muthukumar M. J Chem Phys 2003;118:6648.
[22] Agarwal PK, Somani RH, Weng W, Mehta A, Yang L, Ran S, et al. Macromolecules 2003;36:5226–35.
[23] Liedauer S, Eder G, Janeschitz-Kriegl H, Jerschow P, Geymayer W, Ingolic E. Int Polym Process 1993;8:236.
[24] Liedauer S, Eder G, Janeschitz-Kriegl H. Int Polym Process 1995;3:243.

[25] Avrami M. J Chem Phys 1939;7:1103. Avrami M. J Chem Phys 1940; 8:212. Avrami M. J Chem Phys 1941;9:177.
[26] Sano H, Yiu H, Li H, Inoue T. Polymer 1998;39:5265.
[27] Liu G, Li H. J Appl Polym Sci 2003;89:2628.
[28] Liu G, Chen Y, Li H. J Appl Polym Sci 2004;92:3894.
[29] Ogita T, Kawahara Y, Sawartari C, Ozaki F, Matsuo M. Polym J 1991; 23:871.
[30] Hashmi SAR, Neogi S, Pandey A, Chand N. Wear 2001;247:9.
[31] Sugimoto M, Masabuchi Y, Takimoto J, Koyama K. Macromolecules 2001;34:6056.
[32] Vega JF, Rastogi S, Peters GMW, Meijer HEH. J Rheol 2004;48:663.
[33] Yang L, Somani RH, Sics I, Hsiao B, Kolb R, Fruitwala H, Ong C. Macromolecules 2004;37:4845.
[34] Fraser RDB, Macrae TP, Miller A, Rowlands RJ. J Appl Crystallogr 1976;9:81.
[35] Ruland W. J Appl Crystallogr 1971;4:70.
[36] Sperling LH. Introduction to physical polymer science. USA: Wiley; 2001.
[37] Keum JK, Burger C, Hsiao BS, Somani R, Yang L, Kolb R, et al. Prog Colloid Polym Sci. 2005;130:1.
[38] Ran S, Zong X, Fang D, Hsiao BS, Chu B, Ross R. J Appl Crystallogr 2000;33:1031.
[39] Dean DM, Rebenfeld L, Register RA, Hsiao BS. J Mater Sci 1998;33: 4797.
[40] Auriemma F, de Rosa C, Boscato T, Corradini P. Macromolecules 2001;34:4815.
[41] Jungnickel BJ. In: Reiter G, Sommer U, editors. Lecture notes physics, vol. 606. Springer; 2003. p. 208.
[42] Olabisi O, Robeson LM, Shaw T. Polymer–polymer miscibility. USA: Academic Press; 1979.
[43] Schultz JM. Polymer crystallization. The development of crystalline order in thermoplastic polymers. USA: Oxford University Press; 2001.
[44] Hindawi IA, Higgins JS, Weiss RA. Polymer 1992;33:2522.
[45] Gerard H, Cabral JT, Higgins JS. Phil Trans R Soc Lond A 2003;361: 767.
[46] Jeon HS, Lee JH, Balsar NP, Newstein MC. Macromolecules 1998; 31:3340.
[47] Rajasekaran JJ, Curro JG, Honeycutt JD. Macromolecules 1995;28: 6843.
[48] Li J, Shanks RA, Long Y. Polymer 2001;42:1941.
[49] Lo C-T, Seifert S, Thiyagarajan P, Narasimhan B. Polymer 2004;45: 3671.
[50] de Gennes PG. Scaling concepts in polymer physics. Ithaca, NY: Cornell University Press; 1979.
[51] Doi M, Edwards SF. Theory of polymer dynamics 1986. Oxford, New York.
[52] Milner ST, McLeish TCB. Phys Rev Lett 1998;81:725.
[53] Watanabe H. Prog Polym Sci 1999;24:1253.
[54] desCloizeaux J. Europhys Lett 1988;5:437.
[55] Marucci G. J Polym Sci, Polym Phys Ed 1985;23:159.
[56] Doi M, Graessley WW, Helfand E, Pearson DS. Macromolecules 1987;20:1900.
[57] Park SJ, Larson RG. Macromolecules 2004;37:597.
[58] Terrill NJ, Fairclough PA, Tony-Andrews E, Komanscheck BU, Young RJ, Ryan AJ. Polymer 1998;39:2381.
[59] Monks AW, White HM, Bassett DC. Polymer 1996;37:5933.